



Received Date : 09-Jul-2018
Revised Date : 07-Feb-2019
Accepted Date : 20-May-2019

Structural and functional studies on *Salmonella typhimurium* pyridoxal kinase (PdxK): the first structural evidence for the formation of Schiff base with the substrate

Geeta Deka^{1*}, Josyula N. Kalyani^{2*}, Fathima Benazir J.¹, Pallavi Sabharwal², Handanahal S. Savithri² and Mathur R. N. Murthy^{1#}.

¹ Molecular Biophysics Unit, Indian Institute of Science, Bangalore 560012, India

² Biochemistry Department, Indian Institute of Science, Bangalore 560012, India

* Equal contributions

Correspondence e-mail: mrn@iisc.ac.in , Tel: +91-80-22932310

Running title: Structural and functional studies on *St*PLK

Article type : Original Articles

Keywords: Pyridoxal kinase (PLK), Pyridoxal 5' phosphate (PLP), activity, Schiff base, Pyridoxal (PL), X-ray crystallography

Abbreviations

PLP, pyridoxal 5' phosphate; PLK, pyridoxal kinase; *St*PLK, *Salmonella typhimurium*; ADP, adenosine diphosphate; ATP, adenosine triphosphate; PMN, pyridoxamine; SPR, surface plasmon resonance; PN, pyridoxine; PMN, pyridoxamine; PL, pyridoxal; PNP, pyridoxine 5' phosphate; PMP, pyridoxamine 5' phosphate; PLP, pyridoxal 5' phosphate; PNPOx, pyridoxine (pyridoxamine) 5' phosphate oxidase; DXP, deoxyxylulose 5' phosphate; ALT,

This article has been accepted for publication and undergone full peer review but has not been through the copyediting, typesetting, pagination and proofreading process, which may lead to differences between this version and the Version of Record. Please cite this article as doi: 10.1111/febs.14933

This article is protected by copyright. All rights reserved.

alanine aminotransferase; GAD, glutamate decarboxylase; GTP, guanosine triphosphate; β ME, 2-mercaptoethanol; PEG, polyethylene glycol; RMSD, root mean square deviation; PDB, protein data bank; NADH, Nicotinamide adenine dinucleotide; LDH, lactate dehydrogenase; ELISA, enzyme-linked immunosorbent assay

Abstract

A large number of enzymes depend on the ubiquitous co-factor pyridoxal 5' phosphate (PLP) for their activity. Pyridoxal kinase (PLK) is the key enzyme involved in the synthesis of PLP from the three forms of vitamin B₆ via the salvage pathway. In the present work, we determined the unliganded structure of *St*PLK in a monoclinic form and its ternary complex with bound pyridoxal (PL), ADP and Mg²⁺ in two different tetragonal crystal forms (Form I and Form II). We found that, in the ternary complex structure of *St*PLK, the active site Lys233 forms a Schiff base linkage with the substrate (PL). Although formation of a Schiff base with the active site Lys229 was demonstrated in the *E. coli* enzyme based on biochemical studies, the ternary complex of *St*PLK represents the first crystal structure where the Schiff bond formation has been observed. We also identified an additional site for PLP binding away from the active site in one of the ternary complexes (crystal Form I), suggesting a probable route for the product release. This is the first ternary complex structure where the modelled γ -phosphate of ATP is close enough to PL for the phosphorylation of the substrate. *St*PLK prefers PL over pyridoxamine (PMN) as its substrate and follows a sequential mechanism of catalysis. Surface Plasmon Resonance (SPR) studies suggest that *St*PLK interacts with apo PLP-dependent enzymes with μ M affinity supporting the earlier proposed direct transfer mechanism of PLP from PLK to PLP-dependent enzymes.

Introduction

Pyridoxal kinase (PLK, encoded by PdxK) belongs to the ribokinase superfamily of enzymes and catalyzes the phosphorylation of pyridoxine (PN), pyridoxamine (PMN) and pyridoxal (PL) to their 5' phosphorylated forms, pyridoxine 5' phosphate (PNP), pyridoxamine 5' phosphate (PMP) and pyridoxal 5' phosphate (PLP), respectively (Figure 1). PNP and PMP may subsequently be converted to PLP by pyridoxine (pyridoxamine) 5' phosphate oxidase (PNPOx) [1].

PLP is the cofactor for a large number of enzymes exhibiting a wide range of activity such as transamination, decarboxylation, racemization, elimination and replacement reactions of amino acids and steroids etc [2, 3, 4]. Animals obtain PLP from vitamin B₆ precursors (PL, PN and PMN) via a salvage pathway involving PLK and PNPOx [5]. Prokaryotes, lower eukaryotes and plants can synthesize PLP *de novo* by a deoxyxylulose 5' phosphate (DXP) dependent pathway [6] as well as a DXP independent pathway [7]. Inhibition or malfunction

of PLK/PNPOx or lack of precursor forms of vitamin B₆ might result in PLP deficiency, which is known to cause severe pathologies such as Schizophrenia, Parkinson's, Alzheimer's, Epilepsy etc [5, 8]. PLP concentration can be used as a prognostic parameter in cancer detection [9].

Because of its importance, extensive studies on PLKs from different sources have been carried out. PLK has been purified and characterized from *E. coli* [10], human [11], sheep brain [12], pig liver [13], *Arabidopsis thaliana* [14] and *Bacillus subtilis* [15]. Crystal structures of PLK has been reported from *E. coli* (Kinase 1, [10], Kinase 2, [16]), human [17], sheep brain [18], *Bacillus subtilis* [19] and *Pseudomonas aeruginosa* [20]). These proteins are homodimers with an independent active site in each protomer. It has been proposed that the sheep brain enzyme undergoes conformational changes [21] upon binding of the substrate, which is thought to be necessary for the ATP dependent phosphorylation of PL. However, such changes have not been observed in prokaryotic PLKs. Although, several crystal structures of PLKs have been reported, most structures represent either ATP (or ADP) or PL bound forms. Only in a few structures, ternary complexes have been observed, where either ATP (or ADP) and PL are bound together at the active site. In the ternary complex structures of both in *E. coli* [8] and sheep brain PLK [21], it was observed that the γ -phosphate of ATP is at a distance of $\sim 6 \text{ \AA}$ from the hydroxyl group of PL, a distance not favorable for the phosphorylation of PL. Therefore, it was speculated that during catalysis the γ -phosphate of ATP comes close to the hydroxyl group of PL. Biochemical studies carried out on the *E. coli* enzyme have shown that excess of PLP/PL inhibits the enzyme and it has been demonstrated that this inhibition is a result of the formation of a covalent bond between PL/PLP and an active site Lysine residue, Lys229 [22, 40]. However, no crystallographic evidence has been obtained in earlier studies for the covalent binding of PL/PLP to PLK.

Due to the presence of a highly reactive aldehyde group, it is crucial to tightly regulate the concentration of PLP in cells as higher as well as lower levels of PLP cause cellular toxicity. The mechanism that maintains the PLP homeostasis in cells is not well understood and how PLP is transferred from PLK to apo-PLP dependent enzymes inspite of maintaining its very low ($\sim 1 \mu\text{M}$ in eukaryotes) concentration in cells is still a mystery. One of the proposed mechanisms is that specific interactions could lead to direct transfer of the newly synthesized PLP [23] from PLK to apo-PLP dependent enzymes. Studies on the interactions of eukaryotic PLK (Porcine) with PLP-dependent enzymes, alanine aminotransferase (ALT) and glutamate decarboxylase (GAD) have been carried out earlier

[23]. However, there are no reports demonstrating interactions between prokaryotic PLK (sharing < 30% sequence identity with eukaryotic PLK) and PLP dependent enzymes.

In this paper, we present structural and biochemical investigations on *S. typhimurium* pyridoxal kinase (*St*PLK). The X-ray crystal structures of the unliganded *St*PLK (P2₁2₁2₁) and two different tetragonal (P4₃2₁2) crystal forms (Form I and Form II) of its complex with PL, ADP and Mg²⁺ were determined. The liganded structures suggest that *St*PLK could form a ternary complex in the presence of excess PL, Mg²⁺ and ATP in which PL is covalently attached to Lys233 via a Schiff base linkage. This observation accounts for the observed substrate inhibition of PLK. A second site for the binding of PLP away from the active site and close to the bulk solvent was located for the first time in the crystal structure of one of the ternary complexes, suggesting a probable route for product release. Biochemical studies on the interaction of *St*PLK and PLP dependent enzymes suggest feasibility of a direct transfer of the product PLP.

Results and discussions

Substrate specificity and kinetic mechanism of *St*PLK

Activity of *St*PLK with vitamin B6 derivatives PL, PN and PMN (Table 1) was estimated as described in the materials and methods. *St*PLK showed highest activity for PL at acidic pH (6.2-6.6) and 80% of the activity was lost at alkaline pH (>7). The enzyme was active over 30–50 °C temperature range. *St*PLK was inactive towards PN but significant activity was observed at pH 8.5 with PMN as the substrate, suggesting that the enzyme converts PMN and ATP to PMP and ADP at higher pH. It was observed that *St*PLK prefers Mg²⁺ over Zn²⁺ ion for activity. Other PLKs such as *E. coli* and *T. brucei* PLKs are also known to show higher activity in presence of Mg²⁺ [10, 38] whereas the human and sheep brain PLKs show preference for Zn²⁺ ion [21, 39]. A competition assay was performed at a neutral pH (pH 7.0) where both PL and PMN show measurable kinase activity to identify the preference of *St*PLK between PL and PMN. The results suggested that the enzyme prefers PL over PMN (data not shown). It was observed that *St*PLK cannot use other nucleotides such as GTP as a substrate instead of ATP.

Steady state kinetic method was used to elucidate the reaction mechanism followed by *St*PLK. Initial velocities were measured for the bi-substrate reaction at a fixed concentration of ATP and varying concentrations of PL (0-200 μM). Double-reciprocal plots of 1/v vs 1/[PL] were drawn at fixed concentrations of ATP. Similar experiments were carried out

wherein PL concentrations were fixed and the concentration of ATP (50 μ M - 1 mM) was varied. Using the initial velocities determined, double-reciprocal plots were obtained. The appearance of a converging pattern of lines for both ATP and PL suggests that *St*PLK follows a sequential mechanism (data not shown).

Product inhibition studies

The products of *St*PLK reaction are PLP and ADP. Product inhibition studies could not be carried out with PLP as the added PLP precluded estimation of PLP formed by the reaction. Hence, the reactions were carried out in the presence of the second product, ADP. Initially, the reaction was monitored at saturating concentrations of PL and ATP with increasing concentrations of ADP (0-5 mM). The X-intercept of the resulting Dixon plot, $1/v$ vs. [ADP] (Figure 2A) suggested that the inhibition constant (K_i) of *St*PLK.ADP complex is 1.3 mM. Product inhibition studies were carried out at fixed concentrations of ADP (lower and higher than K_i) with varying concentrations of either PL or ATP and saturating concentration of the other substrate and double reciprocal plots of the data obtained were plotted (data not shown). In both the cases, a set of coincidental lines (non-competitive inhibition), indicating no change in K_m but decreased V_{max} with increase in ADP concentration was observed. Since ADP did not act as a competitive inhibitor for either of the substrates, it is clear that it does not bind to the same form of the enzyme as the substrates. Therefore, the mechanism is likely to be random sequential.

In the kinetic studies, it was observed that only 10% of PL was converted to PLP even in the presence of saturating concentrations of PL and ATP. Similar observation has been reported with *Ec*PLK [22]. In order to examine the effect of the released PLP on the reaction, the kinase reaction was monitored at 388 nm for 5 min using 1mg/ml of *St*PLK. The reaction stopped within 5 min as observed with *Ec*PLK [22]. Addition of a fresh stock of 1mg/ml of *St*PLK resulted in increased PLP formation for an additional 5 min (Figure 2 B). Similar increase was observed when the addition of *St*PLK was repeated, although the increase was lower. This suggested that the enzyme turn-over was reduced due to the formation of the product. This also suggests that the PLP formed might be bound at the active site preventing further binding of the substrate PL as was demonstrated earlier with *Ec*PLK [22]

Structure determination and quality of the models

The structures of native as well as the two ligand bound forms of *St*PLKs were determined by molecular replacement using the program PHASER of CCP4 suite [28]. The asymmetric unit in the native as well as the liganded crystal forms contained two protomers (A and B) related by a non-crystallographic two fold axis of symmetry. The native *St*PLK (space group P2₁2₁2₁) structure was determined at 2.6 Å resolution with a R_{work}/ R_{free} factors of 22.37% and 28.92%, respectively. The liganded crystal Form I diffracted X-rays to 2.4 Å resolution while crystals of Form II diffracted X-rays to 2.2 Å resolution. The R_{work} / R_{free} factors after final refinement of the two crystal forms of the complex are 21.63% / 23.45% and 21.18% / 24.10%, respectively. The data collection and refinement statistics for these structures are listed in Table 2.

Evaluation of the geometry of the final models using the program PROCHECK [31] showed that more than 90% of the residues in all the three structures were in the most favorable regions and no residue was in the disallowed region of the Ramachandran map indicating the accuracy of the refined models. Diffraction data of the unliganded structure suffered from contamination of a small molecule crystal of unknown identity [24] and perhaps for this reason, one residue was found in the disallowed region.

In all the structures, density for 14-16 N-terminal residues and 4-5 C-terminal residues was absent. The residue Cys126 was modified to hydroxyethylthiocysteine in protomer A and B of Form I and Form II crystals. The modification is probably due to the inclusion of βME in the protein purification buffer. However, the modified cysteine residues occur in the solvent exposed region away from the active site and hence their chemical modification is unlikely to have any functional significance. In the native *St*PLK structure, electron density corresponding to three EDO and one PEG 3350 (PE4) was observed, both of which were present in the crystallization condition. The PE4 molecule interacts with Glu47 of protomer B and is involved in hydrogen bonding with a few waters molecules, EDO and residues from a nearby symmetry related dimer. The binding of PE4 is not rare and there more than 100 entries in the PDB with a bound PE4 at protein interfaces.

Comparison of structure of native *St*PLK with its ligand bound forms

*St*PLK crystallized in its dimeric form. The polypeptide fold confirms to the three layered $\alpha\beta\alpha$ sandwich structure found in other ribokinase superfamily of proteins [10, 17, 18]. Each protomer of *St*PLK consists of eight α -helices (H1-H8) and seven β -strands (S1-S7) (Figure 3A). In the native dimeric structure of *St*PLK, a phosphate molecule could be located at the active site of both the protomers (Figure 3B). As inferred from comparison with ATP bound structures of other PLKs (*E. coli*, sheep, human), the bound phosphate occupies the position corresponding to the γ phosphate of ATP [10, 18, 25]. The phosphate is held by hydrogen bonding with atoms in an anion hole formed by a $^{234}\text{GTGD}^{237}$ motif. In protomer A, a Mg^{2+} ion could be located near the bound phosphate. In protomer B, no density for an equivalent Mg^{2+} ion was found; instead a water molecule hydrogen bonded with Tyr141 hydroxyl group could be observed.

No large conformational differences were observed between the unliganded *St*PLK and its two liganded forms (RMSD of $> 1\text{\AA}$). In protomer A of the Form I and Form II ligand bound structures, electron density corresponding to a PL covalently attached to an active site lysine residue (Lys233) forming a Schiff base, an ADP and a Mg^{2+} ion was observed (Figure 4A). PL is stabilized by hydrogen bonding interactions with Ser28, Asp237 and a water molecule. A π - π stacking interaction observed between the PL ring and Tyr101 may also position and orient PL (Figure 4C). The ADP binds in a shallow groove such that the adenine and ribose moieties are buried in a partial hydrophobic pocket. The residues that interact with the nucleotide (Val228, His225, Thr200, and Ser201 in *St*PLK) are conserved within the ribokinase family [10] (Figure 4B). Comparison of the ADP binding of *St*PLK with those of *Ec*PLK and *Sh*PLK shows that the largest deviations in the positions of corresponding atoms are at the phosphate groups. In *St*PLK, the α -phosphate of ADP interacts with Ser201, Thr235 and nearby water molecule. The β phosphate of ADP interacts with Gly236, Asn164, one Mg^{2+} ion and a few water molecules. The Mg^{2+} ion with square pyramidal geometry is bound at a place where the γ -phosphate of ATP has been observed in other PLK structures. The Mg^{2+} ion is coordinated with O3 of the β phosphate ($\sim 2.0\text{\AA}$) and four water molecules. The Mg^{2+} ion has been proposed to be important for stabilizing the β/γ phosphate of the bound ADP/ATP and also probably the reaction intermediates formed during catalysis. In both Form I and Form II *St*PLKs, a water molecule was observed at a position corresponding to that of Mg^{2+} in *Ec*PLK and Zn^{2+} in *Sh*PLK [18, 21]. This water is hydrogen bonded to residues Glu167 (2.67\AA), Tyr141 (2.70\AA) and two other nearby water molecules. In

protomer B of Form I crystal, a non-covalently bound PLP at a site away from the substrate binding site and a Tris molecule occupying a position corresponding to the γ phosphate binding site of ATP in protomer A were observed.

Ligands bound to protomer A in crystal Form II were identical to those bound in Form I. In protomer B of crystal Form II, a Tris molecule equivalent to the Tris bound to protomer B of Form I was observed. The Tris might have come from the crystallization condition. The Tris moiety in both the protomers is hydrogen bonded to Glu167 (2.77 Å), Asp130 (2.74 Å), Thr162 (2.98 Å), Tyr141 (3.19 Å), Thr200 (2.98 Å) and a water molecule. These interactions are similar to those reported for *Ec*PLK [10]. However, no electron density for PLP was observed in protomer B of crystal Form II.

It has been proposed that the active site of *Ec*PLK undergoes a conformational change involving movement of ~ 6 Å upon substrate binding so that the hydroxyl group of PL comes close to the γ phosphate of ATP [10]. However, the position of PL in *St*PLK is different as it is held by covalent bonding with Lys233 and this leads to a movement of ~ 1 Å towards the ATP binding site of *Ec*PLK. This conformational difference observed between *E. coli* and *S. typhimurium* PLKs suggests that the bound substrates (ATP, PL and Mg^{2+}) may have conformational flexibility needed for efficient phosphorylation of PL.

Structural changes associated with Schiff base formation

The active site Lys237 of *E. coli* is conserved in *S. typhimurium* also. The equivalent residue is Val231 (PDB code: 3KEU) in human, Val231 in Sheep (PDB code: 1LHP) and Thr241 in *E. histolytica* (PDB code: 4S1H). Formation of a Schiff base between Lys233 and PL in the presence of excess PL might prevent the formation of excess PLP. This might reduce PLP mediated toxicity in prokaryotes. Eukaryotes/protozoans might follow a different mechanism to prevent PLP mediated toxicity as they do not have a Lys residue in the active site to form Schiff base with PL or PLP. Comparison of the *St*PLK Form I structure with the PL bound *Ec*PLK (PDB code: 2DDW) suggests that the terminal amine group of Lys233 is at ~ 6 Å away from the 4'-hydroxyl group of PL in *Ec*PLK, which is unfavorable for the formation of a Schiff base linkage. However, in the presence of excess PL, Lys233 might undergo a large movement ($\sim 6-8$ Å) leading to the formation of the Schiff base linkage. The PL molecule is stabilized by interactions with nearby His59 and Asp233 in the *E. coli* enzyme. However, formation of the Schiff base in *St*PLK leads to the disruption of interaction of PL with equivalent His64 while retaining the interaction with the Asp237 (Figure 5).

Probable Conformational transitions associated with product (PLP) release

As described earlier, a second site for PLP binding was observed in protomer B of *St*PLK. The pyridine ring of this PLP is stabilized by π - π stacking interactions with Tyr101 and Pro63 and hydrogen bonding interactions with a nearby water molecule (Figure 6B). In protomer A, PL was bound to Lys233 via a Schiff base linkage. Superposition of the protomer A over protomer B suggests that PLP position in protomer B is suitable for product release rather than catalysis (Figure 6A). The aldehyde group of PLP bound to protomer B points towards the surface and hence apo- PLP dependent enzymes might capture the surface exposed PLP leading to PLP-bound enzyme forms. The B-factor for PLP is high ($\sim 75 \text{ \AA}^2$) as compared to the B-factor of the surrounding residues ($\sim 30 \text{ \AA}^2$) indicating that it is held by weak interactions. This favours easy release of PLP from the enzyme. Comparison of the conformations of the product (PLP) bound form with the substrate (ADP and PL) bound form suggests significant conformational changes between these two forms, especially in two loops (Loop I and Loop II). The flexible loop I (residues Gly134-142Val in *St*PLK) has been referred to as a flap or a lid in other ribokinase family proteins (Li *et al*, 2002). These two loops show a displacement of $\sim 2 \text{ \AA}$ between the two complex structures. This displacement might be important for avoiding steric clashes between PLP and Pro63/His64 during product release.

Loop I of *Sh*PLK (residue Gly117-128Val) and *Hs*PLK (residue Gly117-128 Val) are longer than that of *St*PLK (residues Gly134-142Val). Loop I of *Sh*PLK is in a closed conformation when only ADP is bound at the active site but assumes an open conformation when both ADP and PL are bound. Loop I is disordered in the native *Hs*PLK and gets ordered only upon binding of substrates. The shorter loops of *St*PLK or *Ec*PLK, in contrast, are ordered both in the native and ligand bound forms. Also, in contrast to the large conformational change upon ligand binding observed in *Sh*PLK and *Hs*PLK, only marginal changes of 1-1.5 \AA in the position of loop I is observed between native and liganded (ADP, PL and Mg^{2+}) *St*PLK structures. These differences in the conformational features of Loop I may be a result of its different lengths in these structures. The shorter loops of *St*PLK and *Ec*PLK appear to be equivalent to the open conformation observed *Sh*PLK and *Hs*PLK that allows ligand binding.

The conformation of the active site Loop II (residues 60-69 in *St*PLK) has been thought to be important for the function of PLKs. Unlike loop I, the size and conformation of loop II are very similar in *St*PLK, *Ec*PLK, *hs*PLK and *Sh*PLK. Loop II contains the 63Pro-His64 motif involved in hydrogen bonding and hydrophobic interactions with the substrate PL in *Ec*PLK [10]. These interactions were not observed in *St*PLK, probably due to the displacement of PL by 1.4 Å towards ATP resulting from the formation of the Schiff base with Lys233. Also, His64 of loop II may prevent loop I from moving towards the substrate binding site and maintain loop I of *Ec*PLK and *St*PLK in an open state even in the absence of the substrate. The side chain of His64 may also shield the active site from the solvent. The Pro-His sequence has been replaced by Thr-Gln in the pdxY homologs.

Biochemical evidence for PL binding

PL forms a Schiff base linkage with Lys233 in the crystal structure of *St*PLK obtained after co-crystallization with ATP, PL and Mg^{2+} . To confirm the formation of the Schiff base linkage in solution, *St*PLK reaction was monitored spectrophotometrically in the crystallization condition. Addition of 0.3 mM PL to the reaction mixture (1mg/ml *St*PLK, 3 mM ATP in the crystallization buffer) resulted in an increase in the absorbance at 410 nm within 15 sec with a concomitant decrease in absorbance at 325 nm, which corresponds to absorbance maximum of PL. Further incubation of the reaction mixture (upto 10 min) resulted in a gradual increase of absorbance at 410 nm, suggesting the formation of a Schiff base between PL and a Lys. A concomitant decrease in absorbance at 325 nm was also observed, which correlates with the utilization of PL in the catalytic cycle (Figure 7A).

To examine if *St*PLK could form a Schiff base or aldimine linkage with PL in solution, the *St*PLK reaction mixture was subjected to $NaBH_4$ reduction and the UV spectrum was monitored. An increase in the absorbance at 325 nm was observed upon incubation for 10 min, with a concomitant decrease of absorbance at 410 nm, suggesting the reduction of the Schiff base linkage to a diamine (Figure 7B). This further provides support for the formation of a Schiff base in solution.

To further confirm the role of Lys233 in the formation of Schiff base linkage, we mutated Lys233 to Ala (K233A) and carried out biochemical characterization of the mutant. The mutant showed significant loss in activity towards PL and about 14 fold increase in K_m as compared to the wild type enzyme (Table 3, Figure 8A). This suggests that Lys233 is not only important for Schiff base formation but also plays an important role in substrate binding and catalysis. We have shown that in *St*PLK only 10% of PL gets converted to PLP because

of the formation of the Schiff base with Lys233. The kinase reaction for K233A was performed in the same way as with the wild type *St*PLK using 1 mg/ml of the mutant protein. Fresh stock of 1 mg/ml of *St*PLK (K233A) was added to the reaction mixture at the end of 5 min and the reaction was further monitored. Unlike wild type *St*PLK, incubation of *St*PLK (K233A) with the reaction mixture did not reach saturation presumably because the PLP formed could not form Schiff base and inhibit further binding of PL (Figure 8B).

Dimeric structure: asymmetry in ligand binding to the two protomers of *St*PLK

As evaluated using the PISA server [37], the buried interface area of native *St*PLK as well as its liganded forms is in the range of 1575 Å² to 1692 Å² indicating that ligand binding does not induce large changes in the inter-subunit organization of *St*PLK. The large interface area suggests that the dimers are likely to be stable in solution, which is also confirmed by gel filtration studies. Comparable buried interface areas are found in homologous structures of *Ec*PLK, *Hs*PLK etc [10, 17].

In the Form I and Form II crystal structures of liganded *St*PLK, ligands bound to the two protomers (A and B) of the dimer were not identical. In both crystal forms ADP (not ATP) and PL were bound to protomer A whereas these ligands were absent in protomer B. It was of interest to examine whether the asymmetry in ligand binding between the two protomers of the dimer is an intrinsic property of the protein or caused by crystal packing. In crystal Form I, a loop comprising of residues 224-228 is away from the ADP binding site in protomer A providing space for the binding of the ligands. The same loop is closer towards the ADP binding site by about 2 Å due to crystal packing in protomer B. The displacement of this loop (residue 224-228) results in close contacts between His225, Pro226 with a modeled ATP/ADP, which might hinder its binding to protomer B. Thus, the asymmetry observed between the two protomers probably results from differences in crystal packing and unlikely to be an intrinsic property of the dimeric *St*PLK.

Structural implications for catalysis by *St*PLK

In *Ec*PLK, the distance between the γ phosphate of ATP and the pyridoxal binding site is in the range of 6 to 8 Å [10]. At this distance, it would be impossible for a spontaneous transfer of phosphate from ATP to PL. Therefore, some conformational change in the enzyme active site pocket is expected that will bring the γ phosphate of ATP close to PL. Li *et al.*, (2004) [21] hypothesized that there is another state of the protein conformation which they

referred to as the “pre- reaction / transition state”, which might represent the structure just before the phosphate transfer in which the two substrates are close enough for the reaction to occur. The movement of loop I amino acid residues of *St*PLK towards the active site upon ligand binding may lead to such a pre-reaction state. This movement may also lead to stabilization of the ATP γ phosphate by the anion hole ($^{234}\text{GTGD}^{237}$). The interaction of the γ phosphate with the negatively charged glutamate is partially alleviated by a water molecule and the Mg^{2+} . The side chain carboxyl group of Asp237 of the $^{234}\text{GTGD}^{237}$ motif forms a strong hydrogen bond ($\sim 2.9 \text{ \AA}$) with the 5' hydroxyl of PL, enhancing its nucleophilicity. Asp237 is conserved among all PLKs and may initiate the reaction by de-protonation of the hydroxyl group of PL. The deprotonated PL may simultaneously attack the γ phosphate of ATP resulting in the transfer of a proton from the 5' OH to the carboxyl group of Asp237 and concomitant transfer of the γ phosphate to PL. Interestingly, crystal structures of Form I and Form II with ligands (ADP, PL and Mg^{2+}) bound to the protomer A of show that the distance between the β phosphate of ATP and the hydroxyl group of PL is $\sim 4.9 \text{ \AA}$. Modeling ATP in the place of ADP reduces the distance to $\sim 3.3 \text{ \AA}$ and this distance is favorable for the transfer of γ phosphate from ATP to PL leading to PLP. Therefore, the ligand bound structure presented here probably represents the “transition state/pre reaction state” of the enzyme.

Biochemical evidence for interactions of *St*PLK and PLP-dependent enzymes

Presence of free PLP is toxic to the cell as it can bind to free amino acids and lead to metabolic imbalance. It is hypothesized that the toxicity might be reduced by direct transfer of PLP from PLK to the apo forms of the PLP-dependent enzymes. It was demonstrated that eukaryotic (porcine) PLK interacts with two fold type I PLP dependent enzymes, alanine aminotransferase and glutamate decarboxylase (23). Hence, it was of interest to examine if prokaryotic *St*PLK also interacts with PLP dependent enzymes belonging to different folds and functions. Therefore, plausible interaction of *St*PLK with PLP dependent enzymes 2, 3 diamino propionate ammonia lyase (DAPAL) from *E. coli* and *S. typhimurium*, serine hydroxymethyl transferase from *B. streothermophilus* (*Bs*SHMT) and D-cysteine slylhydrolase from *S. typhimurium* (*St*DCytD) was investigated using ELISA based assay.

ELISA based interaction studies were carried out as described in the methods section. The plates were initially coated with the apo or the holo forms of the enzymes, and *St*PLK was added. The bound *St*PLK was estimated by using anti *St*PLK antibodies as primary antibody, The OD at 450 nm with holo and apo enzymes were significantly greater than the negative controls. The OD_{450nm} values obtained with apo forms of the enzymes were

much higher and were comparable to that obtained when *St*PLK was directly coated on the ELISA plate (positive control) (Figure 9A). This suggests that *St*PLK has a higher affinity for interaction with apo enzymes as compared to the holo-enzymes. However because of limitations of ELISA experiment, from this study we can only be confident that *St*PLK interacts with both apo and holo PLP-dependent enzymes.

Significance of *St*PLK –PLP dependent enzyme interaction

Our ELISA study suggests that *St*PLK interacts with PLP-dependent enzymes. To further analyze if such transfer of PLP from one active site to the other could lead to conversion of the apo form to the holo form, the activity of PLP-dependent enzymes was measured in the absence and presence of *St*PLK and its substrates.

We have shown earlier that 10% of PL gets converted to PLP upon incubation of *St*PLK with its substrates. Hence, for reconstitution experiment we used external PLP concentrations in the range of the amount of PLP that would be produced upon *St*PLK reaction. Apo *St*DAPAL (3 μ M) was incubated with *St*PLK (3 μ M) for 10 min at 25 $^{\circ}$ C, followed by the addition of ATP (2 mM), MgCl₂ (0.7mM) and increasing concentrations of PL (50-500 μ M). The reaction was allowed to continue for 10 min and the amount of pyruvate ($\lambda_{330\text{ nm}}$) released was estimated. The assay without incubation with apo *St*DAPAL served as the control. Similarly, apo *Bs*SHMT (3 μ M) was incubated separately with *St*PLK (3 μ M) for 10 min followed by reaction with PL (20-500 μ M), ATP (2 mM) and MgCl₂ (0.7 mM) for 10 min. The SHMT-catalyzed THF independent cleavage of L-*allo*thr was carried out to monitor the restoration of *Bs*SHMT activity. Figure 9 B shows the percent restoration of activity in apo *St*DAPAL after reconstitution with *St*PLK and its substrates or with added free PLP. It was observed that, addition of 50 μ M PL (corresponding to approximately 5 μ M PLP product formed restored the activity by 60 % while reconstitution with 5 μ M PLP resulted in 10% restoration of activity. There was increase in the percent restoration of activity with increase in PL concentration and a maximum of 90% restoration of activity was observed using 200 μ M PL (Corresponding to approximately 20 μ M PLP). Although there was increase in the restoration of activity upon increasing the concentration of added free PLP, the maximum percent restoration was 70% when 50 μ M PLP was added to apo *St*DAPAL. Similar experiments conducted using apo *Bs*SHMT showed that addition of 50 μ M PL in the *St*PLK reaction resulted in ~80 % regain of activity in the reconstituted apo *Bs*SHMT and increase in concentration of PL (50-100 μ M) resulted in 95% restoration of

activity (Figure 9C). On the other hand, addition of free PLP (10-50 μM) resulted in < 70% regain of activity and addition of 100 μM PLP showed 85% regain of activity. These results suggest that the apo PLP-dependent enzymes can be reconstituted by the PLP formed in *St*PLK reaction much more efficiently when compared to the non-enzymatic reconstitution with externally added PLP.

Surface plasmon resonance (SPR)

Surface plasmon resonance (SPR) experiments were also carried out to monitor the interactions between *St*PLK and apo and holo forms of *St*DAPAL. The data obtained from SPR experiments fitted a simple one-to-one binding model and the dissociation rate constants were calculated. The fitted kinetic values for *St*PLK-holo DAPAL and *St*PLK-apo DAPAL from both *E. coli* and *S. typhimurium* are summarized in Table 4. The equilibrium dissociation constants (K_D) were comparable for all the four enzymes and the binding affinity is higher for apo- enzyme as compared to the holo-form. These results also suggest that PLP transfer from PLK to PLP dependent enzymes may depend on direct interaction between the two enzymes.

Conclusions

Pyridoxal kinase is an important enzyme in PLP salvage pathway. *St*PLK is a biological dimer with one independent active site in each protomer. The enzyme can phosphorylate both PL and PMN, but at different pH. However, the preferred substrate is PL. Binding of ligands induces small conformational changes at the active site, which might be important for efficient transfer of phosphate from ATP to PL. In the presence of excess substrate (PL), the enzyme forms a Schiff base with an active site Lysine (Lys233) leading to the substrate inhibition of the enzyme. This might prevent synthesis of excess PLP, which is toxic to the cell. Comparison of ligand bound *St*PLKs and its closest homologue *Ec*PLK as well as distant homologues such as sheep brain and human PLKs revealed that the bound PL approaches ATP during catalysis. Although ATP could not be trapped at the active site, it was possible to show that an ATP modelled in the place of the bound ADP (in both Form I and Form II), the γ phosphate of ATP will be at a hydrogen bonding distance from the hydroxyl group of PL, a distance suitable for phosphate transfer to PL leading to the product PLP. The asymmetry in terms of ligand binding observed between the two protomers of

*St*PLK dimer is likely to be an artifact of crystal packing. The structures also provide insights on the role of three loops in ligand binding and catalysis. A PLP molecule facing the solvent at a distinct site and held by weak interactions in the protomer B of one of the ligand bound structures (Form I) might represent the product release site of the enzyme. The K_D values obtained from SPR experiment suggest that DAPAL from both *E. coli* and *S. typhimurium* interact with *St*PLK with μ M affinity and interaction is higher for apo-enzymes as compared to the holo form. The product PLP of PLK catalyzed reaction might be directly transferred to some apo PLP-dependent enzymes. This might prevent excess PLP mediated toxicity.

Materials and Methods

Purification, crystallization and X-ray diffraction data collection

*St*PLK was cloned, over-expressed and purified as described previously [24]. The full length protein (~294 amino acids) was purified as a dimer of molecular weight of ~ 68 KDa as suggested by gel filtration studies.

Crystals of the native *St*PLK belonging to the orthorhombic space group $P2_12_12_1$ were obtained by the microbatch method under a condition consisting of 20% (w/v) PEG 4000, 10% (v/v) 2-propanal, 100 mM HEPES pH 7.5 at 293 K as reported earlier [24]. Soaking experiments to obtain ligand bound complexes (PL, Mg-ATP) of the native orthorhombic crystals failed as the crystals dissolved immediately in the native crystallization condition with added ligands. Multiple co-crystallization attempts with ATP, Mg, and PL under the condition that had yielded native crystals were also unsuccessful. However, two crystal forms of *St*PLK complexed with ligands (Form I and Form II) could be obtained using the microbatch method from a droplet containing 5 mg/ml *St*PLK, 50% PEG 4K, 10% glycerol, 100 mM Tris (pH 8.5), 100 mM Na-acetate, 1 mM PL, 1 mM Mg-ATP and 40 mM $MgSO_4$. Both these crystal forms belonged to the tetragonal ($P4_32_12$) space group with similar cell parameters (cell edges are 72.26Å, 72.26Å, 244.88Å for Form I and 73.70Å, 73.70Å, 248.31Å for Form II).

The crystals were soaked in the crystallization condition containing 20% PEG 3350 for the native crystals and 15 % ethylene glycol for the ligand bound crystals as the cryo-protectant before X-ray diffraction data collection. The data were collected at a temperature of 100 K maintained by a stream of nitrogen gas. The diffraction data from native orthorhombic ($P2_12_12_1$) crystals were recorded using a Rigaku RU200 rotating anode X-ray

generator equipped with a Mar345 imaging plate detector system whereas data on the tetragonal (P4₃2₁2) crystals were recorded using a CCD image plate detector at the beam line BM14 of ESRF, Grenoble.

Construction and purification of K233A mutant

Single site mutants of *St*PLK targeting the residue Lys233 was constructed by site directed mutagenesis. The wild type *St*PLK inserted in pET – 22b(+) was used as the template for the generation of the mutant. The forward and reverse primers used for the construction of the mutant are: TG GCG ACG GAG TTA **GCA** GGG ACG GGA GATCT and AGATCTCCCGTCCCTGCTAACTCCGTCGCCA, respectively. The site of mutation is underlined and highlighted in bold. The mutation was further confirmed by sequencing. The mutant was over-expressed and purified as described previously [24].

X-ray data processing, structure solution and analysis

X-ray diffraction data sets were processed and scaled using *iMOSFLM* [25] and *AIMLESS* [26], respectively, of the CCP4 suite of programs [27]. As revealed by the calculation of Matthews coefficient, the number of protomers in the asymmetric unit of both the native and liganded crystal forms was two. The native structure of *St*PLK was determined by the molecular replacement method using the program PhaserMR [28] and *E. coli* PLK (68% sequence similarity, PDB code: 2DDM) as the phasing model [24]. The structures of the ligand bound crystals were determined by molecular replacement using the native *St*PLK structure as the phasing model. The hetero atoms and water molecules were removed from the native *St*PLK while using it as the search model. The structures were improved by several cycles of manual model building using COOT [29] and refinement using REFMAC5 of CCP4 suite [30]. The waters were added to the final refined model both manually (where significant density in the $2Fo-Fc$ map countered at 1σ and $Fo-Fc$ map contoured at 3σ was present) as well as by using the automated water placing option of CCP4. Strong positive densities ($Fo-Fc$ map) at certain positions of the native as well as co-crystallized structures were observed and fitted with appropriate ligands or compounds. The final native protein contains two polypeptide chains, two phosphate molecules, one Mg²⁺ ion, one PEG3350 and 196 water molecules. The crystal Form I contains two polypeptide chains, one ADP, one PL (bound to Lys233), one Mg²⁺ ion, one Tris ion and 294 water molecules. The crystal form II contains two polypeptide chains, one ADP, one PL (bound to Lys233), one Mg²⁺ ion, one

PLP molecule and 315 water molecules. Cys394 in both the protomers in the native monoclinic form as well as the ligand bound tetragonal forms was found to be modified to hydroxyethylthiocysteine. The geometries of all the residues were examined using the program PROCHECK of CCP4 suite [31].

The program ALIGN [32] and SSM [33] superpose of COOT were used for structural alignment and calculation of root mean square deviation (RMSD) between corresponding C α atoms of different structures. The structural homologues of *St*PLK were identified in the PDB using the DALI server [34]. PISA [35] was used for the calculation of buried surface area as well as identification of interfacial residues. The average B-factors of amino acid residues, ligand and water molecules were calculated using the BAVERAGE program of CCP4 suite.

Activity measurements of *St*PLK

Initial velocity measurements for the reaction catalyzed by *St*PLK (PL+ATP \rightarrow PLP + ADP) were carried out spectrophotometrically using a Jasco UV-VisibleV-530 spectrophotometer. The activity was determined using ΔOD_{388} and assuming molar extinction coefficient of PLP to be $6600 \text{ M}^{-1} \text{ cm}^{-1}$. One unit of activity was considered as the nmoles of PLP formed per min. Assays were carried out in 40 mM potassium phosphate buffer (pH 6.6) containing 10 $\mu\text{g/ml}$ *St*PLK and 0.7 mM MgCl_2 and varied concentrations of PL (0-0.2 mM) or ATP (0-1.5 mM) in the presence of fixed concentrations of ATP (1 mM) or PL (0.1 mM), respectively. The Lineweaver-burk plots were drawn to determine the K_m and V_{max} . Activity towards PMN was measured using 20 $\mu\text{g/ml}$ of *St*PLK at pH 8.5 using molar extinction coefficient for PMP at 326 nm (λ_{max}) to be $8300 \text{ M}^{-1} \text{ cm}^{-1}$. The Michaelis-Menten kinetics with PMN and ATP as substrates was carried out and the kinetic parameters were obtained from the double-reciprocal plots. The activity of the K233A mutant was also carried out using the same method except that the PL concentration was varied from 0-2 mM.

Estimation of activities of PLP-dependent enzymes

The activities of PLP dependent enzymes *S. typhimurium* and *E. coli* diaminopropionate ammonia lyase (*St/Ec*DAPAL) were carried out in 1 ml of reaction mixture at 37 $^{\circ}\text{C}$ for 5 min as described earlier [36]. The activity of *Bacillus subtilis* serine hydroxymethyl transferase (*Bs*SHMT) was measured in terms of tetrahydrofolate (THF)-independent cleavage of L-allothrionine to glycine and acetaldehyde as described earlier [37].

The assay mixture contained the enzyme (0.022 nmoles), NADH (0.26 μ M) and LDH (1.5 U) in 20 mM potassium phosphate buffer (pH 7.4).

Inhibition Studies

0.9 μ M *St*PLK was added to 400 μ L reaction mixture containing 1 mM ATP, 0.2 mM $MgCl_2$, and 1 mM PL at 37 °C and the formation of PLP was followed at 388 nm. The reaction was followed in the presence of various concentrations of ADP (0-3 mM). The K_i of ADP was determined from a Dixon Plot. Inhibition kinetics was studied by varying the concentrations of PLP and PL.

Sodium borohydride reduction of PLK Schiff base

*St*PLK (1 mg/ml) was incubated with PL (0.3 mM) and $MgCl_2$ (1 mM) for 10 min in a buffer containing 10 mM Tris-HCl (pH 8.5) and the spectrum was recorded at a wavelength range of 300-500 nm. Then to the same reaction mixture 3 mM ATP was added and spectra were recorded at 15sec, 1, 5 and 10 min of interval, respectively. After sometime 1 mM $NaBH_4$ was added to the same reaction mixture and spectra were recorded in the same wavelength range at a time interval of 15 sec, 1, 5 and 10 min, respectively.

Preparation of apo-PLP dependent enzymes

The apo forms of the PLP dependent enzymes were prepared by treatment with D-cycloserine (DCS). PLP dependent enzymes *St/Ec*DAPAL, *Bs*SHMT, *St*DcytD (1 mg/ml) were individually incubated with 10 mM DCS for 30 min. The PLP-DCS adduct was separated from the enzyme using centricon (Millipore) filtration by spinning at 3000 rpm for 2 h with constant addition of 20 mM potassium phosphate buffer (pH 7.4). The retentate was collected and the absorbance spectrum in the visible range (300-500 nm) was monitored to confirm complete removal of PLP and formation of the apo enzyme.

Examination of apo PLP dependent enzymes activation

The reconstitution and activity measurements with the apo PLP dependent enzymes were carried out to examine if the PLP formed in the *St*PLK reaction could get transferred to the active site of the apo enzymes leading to their activation. Initially, apo *St*DAPAL (3 μ M) was incubated with increasing concentrations of PLP (5-50 μ M) for 10-15 min. 5 μ g of the reconstituted *St*DAPAL was used in a NADH coupled assay to monitor the amount of pyruvate formed. The assay carried out with PLP in the absence of the enzyme was

considered as the blank. Apo *St*DAPAL (3 μ M) was incubated with *St*PLK (3 μ M) for 10 min at $\sim 25^{\circ}\text{C}$, followed by the addition of ATP (2 mM), MgCl_2 (0.7 mM) and increasing concentrations of PL (50-500 μ M). The reaction was allowed to continue for 10 min. 5 μ g of reconstituted apo *St*DAPAL was used for the NADH coupled assay and the amount of pyruvate released was estimated. The assay without incubation with apo *St*DAPAL served as the negative control.

ELISA based protein-protein interaction assay

The ELISA plate wells were coated with BSA or PLP-dependent enzymes (30 nM, 100 μ l) and blocked with 5% skimmed milk (350 μ l) for 1 h. 30 nM of *St*PLK was added and incubated for 2 h. Unbound protein was removed by washes with 1xPBST (PBS with 0.05% Triton-X100). All the wells were incubated for 1 h with primary polyclonal antibodies raised against recombinant *Ec*DAPAL (100 μ l, 1:5000), followed by 1 h incubation with secondary antibodies (100 μ l, Goat anti-rabbit IgG, 1:10000) coupled to horse radish peroxidase (HRP). Addition of substrate ($\text{TMB-H}_2\text{O}_2$) resulted in blue color and the reaction was arrested by the addition of 2 N HCl, which resulted in the appearance of yellow colour (450 nm). Direct-antigen coating ELISA using apo and holo *St*DAPAL served as positive controls. BSA was added as the second protein (30 nM) and the assay in the absence of the second protein was used as the negative control. All the dilutions were made in 1x PBS. Spectramax 340PC384 plate reader was used for the measurements. The same procedure was used while doing ELISA for *Bs*SHMT and *St*DcytD as well.

Determination of binding constant (K_D) using surface plasmon resonance (SPR)

Standard amine coupling method was used to study the interaction between *St*PLK and PLP-dependent enzymes *Ec/St*DAPAL (apo and holo forms). *St*PLK was immobilized on a research-grade CM5 sensor chip (GE healthcare) pre-coated with carboxymethyl and experiments were carried out using a Biacore 3000 optical biosensor (Biacore, Uppsala, Sweden) at 25°C . The carboxymethyl dextran surface on the CM5 sensor chip was first charged by adding NHS and EDC in the ratio of 1:1 and then 1 nM of protein in 10 mM acetate buffer pH 4.0 was injected over the activated surface till a response unit (RU) of above five hundred was observed. Blocking of the charged sensor channel was carried out by the addition of 1 M of ethanolamine. A similar method was used to activate and deactivate the control channel, except for the absence of the protein in the coupling buffer. Analyte concentration ranging from 25-100 μ M was used for the apo and the holo *Ec*DAPAL to

monitor the strength of their interaction with *St*PLK. Similarly, for the apo and the holo *St*DAPAL, the concentration ranges used were 5-20 μ M and 5-25 μ M, respectively. A constant flow rate of 30 μ l/min of buffer containing 1X PBS (pH 7.5) and P20 (0.05%) was used to measure the association and dissociation between the ligand (*St*PLK) and the analyte (apo and holo *St/Ec*DAPAL) for a time period of about 5 mins. Analysis of the sensograms were carried out using the BIA EVALUATION 3.1 software and data were fitted globally to 1:1 Langmuir interaction model and the data quality was assessed by χ^2 value as well as the degree of randomness of the residual plot.

Accession numbers

The co-ordinates as well as structure factors of the native and the ligand bound structures of *St*PLK have been deposited in the PDB under the accession codes 5ZW9, 5ZWA and 5ZWB.

Acknowledgements

The authors gratefully acknowledge Department of Biotechnology (BT/PR7021/BRB/10/1142/2012) and Department of Science and Technology (SR/S2/JCB-12/2005/9.5.2006), Government of India for financial support. MRN and HSS thank J.C. Bose fellowships and the Indian National Science Academy for supporting the work. GD and JNK were supported by IISc fellowships. FB was supported by a Kothari post-doctoral fellowship. The authors used MBU, IISc home source X-ray facility as well as BM14 synchrotron facility at ESRF, Grenoble for data collection.

Author's contribution

MRNM and HSS supervised the work and provided resources. The crystallographic work was planned and carried out by GD and JFB. The biochemical characterization of *St*PLK was carried out by JNK. GD performed the analysis of the structures and wrote the manuscript. PS has carried out the mutant (K233A) kinetics.

Conflicts of interest

There are no conflicts of interest to declare.

References

1. McCormick DB, Chen H (1999) **Update on interconversions of vitamin B-6 with its coenzyme.** *The Journal of nutrition*, **129**(2):325-327.
2. Eliot AC, Kirsch JF (2004) **Pyridoxal phosphate enzymes: mechanistic, structural, and evolutionary considerations.** *Annual review of biochemistry* 2004, **73**(1):383-415.
3. Percudani R, Peracchi A (2003) **A genomic overview of pyridoxal-5'phosphate dependent enzymes.** *EMBO reports*, **4**(9):850-854.
4. Shetty KT, Gaitonde BB (1980) **Effect of contraceptive steroids on γ -aminobutyric acid metabolism and pyridoxal kinase activity in rat brain.** *Experimental neurology*, **70**(1):146-154.
5. di Salvo ML, Contestabile R, Safo MK (2011) **Vitamin B6 salvage enzymes: mechanism, structure and regulation.** *Biochimica et Biophysica Acta (BBA)-Proteins and Proteomics*, **1814**(11):1597-1608.
6. Laber B, Maurer W, Scharf S, Stepusin K, Schmidt FS (1999) **Vitamin B6 biosynthesis: formation of pyridoxine 5'-phosphate from 4-(phosphohydroxy)-l-threonine and 1-deoxy-d-xylulose-5-phosphate by PdxA and PdxJ protein.** *FEBS letters*, **449**(1):45-48.
7. Burns KE, Xiang Y, Kinsland CL, McLafferty FW, Begley TP (2005) **Reconstitution and biochemical characterization of a new pyridoxal-5' phosphate biosynthetic pathway.** *Journal of the American Chemical Society*, **127**(11):3682-3683.
8. Bahi-buisson N, Dulac O (2013) **Epilepsy in inborn errors of metabolism.** In: *Handbook of clinical neurology*. vol. 111: Elsevier: 533-541.
9. Galluzzi L, Vacchelli E, Michels J, Garcia P, Kepp O, Senovilla L, Vitale I, Kroemer G (2013) **Effects of vitamin B6 metabolism on oncogenesis, tumor progression and therapeutic responses.** *Oncogene*, **32**(42):4995.
10. Safo MK, Musayev FN, di Salvo ML, Hunt S, Claude J-B, Schirch V (2006) **Crystal structure of pyridoxal kinase from the *Escherichia coli* pdxK gene: implications for the classification of pyridoxal kinases.** *Journal of bacteriology*, **188**(12):4542-4552.
11. Hanna MC, Turner AJ, Kirkness EF (1997) **Human pyridoxal kinase cDNA cloning, expression, and modulation by ligands of the benzodiazepine receptor.** *Journal of Biological Chemistry*, **272**(16):10756-10760.
12. Maras B, Valiante S, Orru S, Simmaco M, Barra D, Churchich JE (1999) **Structure of pyridoxal kinase from sheep brain and role of the tryptophanyl residues.** *Journal of protein chemistry*, **18**(3):259-268.
13. Tagaya M, Yamano K, Fukui T (1989) **Kinetic studies of the pyridoxal kinase from pig liver: slow-binding inhibition by adenosine tetraphosphopyridoxal.** *Biochemistry*, **28**(11):4670-4675.
14. Lum H-K, Kwok F, Lo SC (2002) **Cloning and characterization of *Arabidopsis thaliana* pyridoxal kinase.** *Planta*, **215**(5):870-879.
15. Newman JA, Das SK, Sedelnikova SE, Rice DW (2006) **Cloning, purification and preliminary crystallographic analysis of a putative pyridoxal kinase from *Bacillus subtilis*.** *Acta Crystallographica Section F: Structural Biology and Crystallization Communications*, **62**(10):1006-1009.
16. Safo MK, Musayev FN, Hunt S, di Salvo ML, Scarsdale N, Schirch V (2004) **Crystal structure of the PdxY Protein from *Escherichia coli*.** *Journal of bacteriology*, **186**(23):8074-8082.

17. Cao P, Gong Y, Tang L, Leung Y-C, Jiang T (2006) **Crystal structure of human pyridoxal kinase.** *Journal of structural biology*, **154**(3):327-332.
18. Li MH, Kwok F, An XM, Chang WR, Lau CK, Zhang JP, Liu SQ, Leung YC, Jiang T, Liang DC (2002) **Crystallization and preliminary crystallographic studies of pyridoxal kinase from sheep brain.** *Acta Crystallographica Section D: Biological Crystallography*, **58**(9):1479-1481.
19. Newman JA, Das SK, Sedelnikova SE, Rice DW (2006) **The crystal structure of an ADP complex of *Bacillus subtilis* pyridoxal kinase provides evidence for the parallel emergence of enzyme activity during evolution.** *Journal of molecular biology*, **363**(2):520-530.
20. Kim MI, Hong M (2016) **Crystal structure and catalytic mechanism of pyridoxal kinase from *Pseudomonas aeruginosa*.** *Biochemical and biophysical research communications*, **478**(1):300-306.
21. Li M-h, Kwok F, Chang W-r, Liu S-q, Lo SCL, Zhang J-p, Jiang T, Liang D-c (2004) **Conformational changes in the reaction of pyridoxal kinase.** *Journal of Biological Chemistry*, **279**(17):17459-17465.
22. Ghatge MS, Contestabile R, di Salvo ML, Desai JV, Gandhi AK, Camara CM, Florio R, González IN, Parroni A, Schirch V (2012) **Pyridoxal 5' phosphate is a slow tight binding inhibitor of *E. coli* pyridoxal kinase.** *PloS one*, **7**(7):e41680.
23. Cheung P-Y, Fong C-C, Ng K-T, Lam W-C, Leung Y-C, Tsang C-W, Yang M, Wong M-S (2003) **Interaction between Pyridoxal Kinase and Pyridoxal-5' phosphate Dependent Enzymes.** *Journal of biochemistry*, **134**(5):731-738.
24. Deka G, Kalyani JN, Benazir JF, Savithri HS, Murthy MRN (2014) **Successful data recovery from oscillation photographs containing strong polycrystalline diffraction rings from an unknown small-molecule contaminant: preliminary structure solution of *Salmonella typhimurium* pyridoxal kinase (PdxK).** *Acta Crystallographica Section F: Structural Biology Communications*, **70**(4):526-529.
25. Battye TGG, Kontogiannis L, Johnson O, Powell HR, Leslie AGW (2011) **iMOSFLM: a new graphical interface for diffraction-image processing with MOSFLM.** *Acta Crystallographica Section D: Biological Crystallography*, **67**(4):271-281.
26. Evans PR, Murshudov GN (2013) **How good are my data and what is the resolution?** *Acta Crystallographica Section D: Biological Crystallography*, **69**(7):1204-1214.
27. Winn MD, Ballard CC, Cowtan KD, Dodson EJ, Emsley P, Evans PR, Keegan RM, Krissinel EB, Leslie AGW, McCoy A (2011) **Overview of the CCP4 suite and current developments.** *Acta Crystallographica Section D: Biological Crystallography*, **67**(4):235-242.
28. McCoy AJ, Grosse-Kunstleve RW, Adams PD, Winn MD, Storoni LC, Read RJ (2007) **Phaser crystallographic software.** *Journal of applied crystallography*, **40**(4):658-674.
29. Emsley P, Lohkamp B, Scott WG, Cowtan K (2010) **Features and development of Coot.** *Acta Crystallographica Section D: Biological Crystallography*, **66**(4):486-501.
30. Murshudov GN, Skubák P, Lebedev AA, Pannu NS, Steiner RA, Nicholls RA, Winn MD, Long F, Vagin AA (2011) **REFMAC5 for the refinement of macromolecular crystal structures.** *Acta Crystallographica Section D: Biological Crystallography*, **67**(4):355-367.
31. Laskowski RA, MacArthur MW, Moss DS, Thornton JM (1993) **PROCHECK: a program to check the stereochemical quality of protein structures.** *Journal of applied crystallography*, **26**(2):283-291.

32. Cohen GH (1997) **ALIGN: a program to superimpose protein coordinates, accounting for insertions and deletions.** *Journal of applied crystallography*, **30**(6):1160-1161.
33. Krissinel E, Henrick K (2004) **Secondary-structure matching (SSM), a new tool for fast protein structure alignment in three dimensions.** *Acta Crystallographica Section D: Biological Crystallography*, **60**(12):2256-2268.
34. Holm L, Rosenström Å, Åkesson P (2010) **Dali server: conservation mapping in 3D.** *Nucleic acids research*, **38** (suppl_2):W545-W549.
35. Krissinel E, Henrick K (2007) **Inference of macromolecular assemblies from crystalline state.** *Journal of molecular biology*, **372**(3):774-797.
36. Khan F, Jala VR, Rao NA, Savithri HS (2003) **Characterization of recombinant diaminopropionate ammonia-lyase from *Escherichia coli* and *Salmonella typhimurium*.** *Biochemical and biophysical research communications*, **306**(4):1083-1088.
37. Jala VR, Prakash V, Rao NA, Savithri HS (2002) **Overexpression and characterization of dimeric and tetrameric forms of recombinant serine hydroxymethyltransferase from *Bacillus stearothermophilus*.** *Journal of biosciences*, **27**(3):233-242.
38. Jones DC, Alphey MS, Wyllie S, Fairlamb AH (2012) **Chemical, genetic and structural assessment of pyridoxal kinase as a drug target in the African trypanosome.** *Molecular microbiology*, **86**(1):51-64.
39. Musayev FN, Di Salvo ML, Ko TP, Gandhi AK, Goswami A, Schirch V, Safo MK (2007) **Crystal structure of human pyridoxal kinase: Structural basis of M⁺ and M²⁺ activation.** *Protein Science*, **16**(10):2184-2194.
40. di Salvo ML, Nogués I, Parroni A, Tramonti A, Milano T, Pascarella S, Contestabile R.(2015) **On the mechanism of *Escherichia coli* pyridoxal kinase inhibition by pyridoxal and pyridoxal 5'-phosphate.** *Biochim Biophys Acta*. Sep;**1854**(9):1160-6.

Table 1 Kinetic parameters of *St*PLK with PL, PMN and ATP as substrates.

Substrate	K_m (μM)	V_{max} (nmoles/min/mg)	k_{cat} (min^{-1})
PL	44 ± 5	200 ± 6	6.4 ± 0.2
ATP (PL)	100 ± 8	200 ± 7	6.4 ± 0.2
PMN	60 ± 3	180 ± 5	5.8 ± 0.3
ATP (PMN)	120 ± 2	180 ± 4	5.8 ± 0.3

*Kinetic parameters were determined from double-reciprocal plots with PL, ATP and PMN as substrates. The reaction for PL and ATP were carried out at pH 6.6 and that for PMN and ATP were carried out at pH 8.5. The assays were carried out in duplicate with three different independent preparations of the enzyme.

Table 2. Data collection, processing and refinement statistics of *St*PLK in its native and two different ligand bound forms (Form I and Form II)

Values in parentheses are for the highest resolution shell.

Parameter	Native <i>St</i> PLK	Form I: <i>St</i> PLK bound to PL-Mg-ADP (A subunit) and product PLP (B subunit)	Form II: <i>St</i> PLK bound to PL-Mg-ADP (A subunit) and Tris (B subunit)
PDB ID	5ZW9	5ZWA	5ZWB
X-ray source	CuK α	CuK α	BM14
Data collection temperature (K)	100	100	100
Wavelength (\AA)	1.5417	1.5417	0.97625
Space group	P2 ₁ 2 ₁ 2 ₁	P4 ₃ 2 ₁ 2	P4 ₃ 2 ₁ 2
Unit cell parameters (a, b, c)	65.11, 72.89, 107.52	72.26, 72.26, 244.88	73.70, 73.70, 248.31
Resolution limits (\AA)	72.89-2.60	62.23- 2. 45	39.94- 2.20
No. of measurements	81,619 (12,715)	350,525 (51,547)	485,981(76,707)
No of unique reflections	14,688 (2274)	23,479 (3297)	36,036 (5152)
Redundancy	5.6 (5.6)	14.9 (15.6)	14.4 (15.3)
$\langle I \rangle / \langle \sigma I \rangle$	9.9 (3.5)	14.9 (5.5)	15.5 (5.8)
Completeness (%)	90.1 (98.1)	94.3 (93.0)	100 (100)

CC _{1/2}	0.99 (0.84)		
† <i>R</i> _{sym} (%) ^b	0.13 (0.48)	0.13 (0.49)	0.11 (0.46)
Refinement			
‡ <i>R</i> _{work} / <i>R</i> _{free} (%)	22.37/28.92	21.63/23.45	21.18/24.10
RMS deviations			
Bond length (Å)	0.0054	0.0041	0.004
Bond angles (°)	1.03	0.9032	0.8850
Average B factors (Å ²)			
Protein atoms	33.70	29.45	32.75
Water atoms	26.75	35.52	40.21
Other hetero atoms	42.68	37.85	43.75
Ramachandran plot (%)			
Most favored	90.8	98.0	91.0
Additionally allowed	9.0	2	9.0
Disallowed	0.2	0.0	0
Number of atoms			
Protein	3940	3946	4119
Water	167	263	322
Ligands	49	127	106

† $R_{\text{merge}} = \frac{\sum_{hkl} \sum_i |I_i(hkl) - \langle I(hkl) \rangle|}{\sum_{hkl} \sum_i I_i(hkl)}$, where, $I_i(hkl)$ is the intensity of the i^{th} observation of reflection hkl , $\langle I(hkl) \rangle$ is its mean intensity and N is the number of measurements (redundancy)

‡ $R_{\text{work}} (\%) = \frac{(\sum_{hkl} |F_o - F_c|)}{\sum_{hkl} F_o}$, where F_o and F_c are observed and calculated structure factors; $R_{\text{free}} (\%)$ is calculated as for R_{work} where randomly selected 5% of the dataset were excluded in refinement process.

Table 3: Comparison of kinetic constants of K233A mutant with the wild type *St*PLK

Protein	Substrate	K_m (μM)	V_{\max} (nmoles/min/mg)	K_{cat} (min^{-1})
<i>St</i> PLK	PL	44 ± 5	200 ± 6	6.4 ± 0.2
<i>St</i> PLK (K233A)	PL	530 ± 10	15.5 ± 1.6	0.496 ± 0.02

Kinetic parameters were determined using Line weaver Burk plots with varying concentration of PL and fixed concentration of ATP (1 mM). 10 $\mu\text{g/ml}$ of both the proteins were used for the assay. For the wild type *St*PLK, PL was varied from 0-200 μM , while for *St*PLK (K233A), PL was varied from 0-2 mM (as the reaction did not reach saturation with 200 μM of PLP) to determine the kinetic constants. The assays were carried out in duplicate with three different independent preparations of the enzyme.

Table 4. The association and dissociation rate constants and equilibrium affinity constants of *St*PLK and apo and holo forms of *St/Ec*DAPAL.

	k_a ($\text{M}^{-1}\text{s}^{-1}$)	K_d (s^{-1})	K_A (M^{-1})	K_D (M)	χ^2
Holo- <i>Ec</i> DAPAL	8.29×10^2	3.53×10^{-3}	3.27×10^5	4.44×10^{-6}	9.88
Apo- <i>Ec</i> DAPAL	5.98×10^2	3.47×10^{-4}	1.84×10^6	5.75×10^{-7}	3.55
Holo- <i>St</i> DAPAL	1.11×10^3	1.47×10^{-3}	7.68×10^5	1.37×10^{-6}	2.93
Apo- <i>St</i> DAPAL	1.14×10^3	4.91×10^{-3}	1.35×10^6	7.64×10^{-7}	1.81

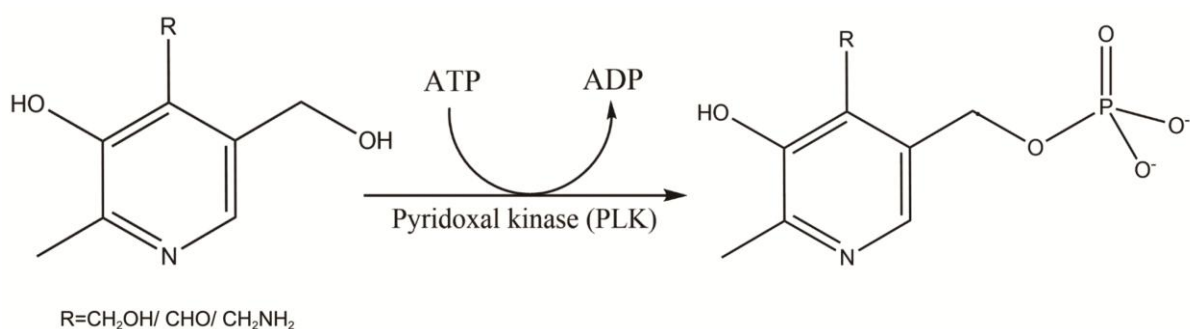


Figure 1. Reaction catalyzed by pyridoxal kinase (PLK). The chemical identity of the ‘R’ group defines the nature of the substrate.

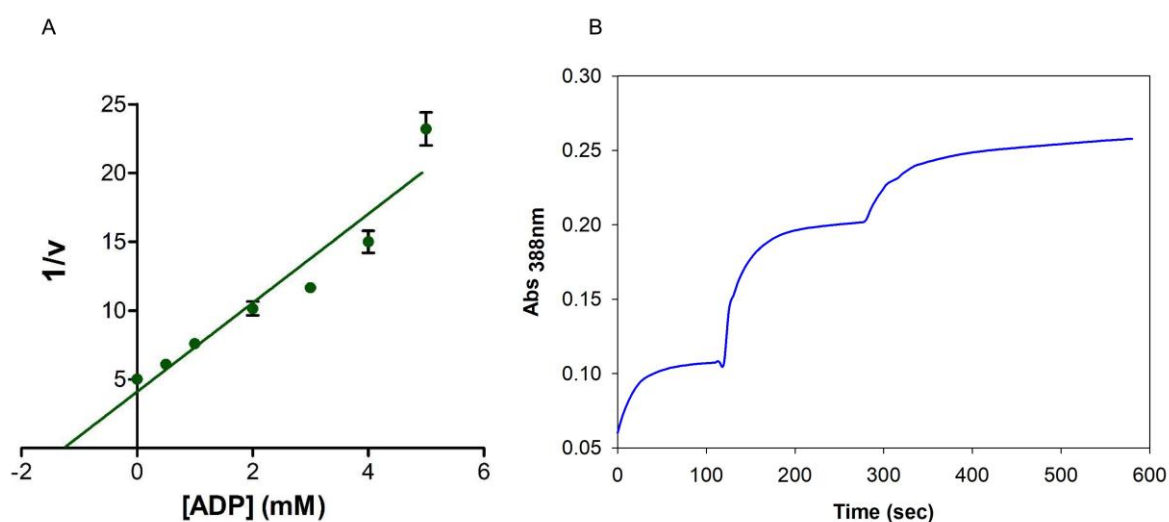


Figure 2. Product inhibition studies on *St*PLK using ADP. (A) Dixon plot ($1/v$ vs. $[ADP]$) obtained by measuring activity in the presence of increasing concentrations of ADP (0, 0.5, 1, 2, 3, 4 and 5 mM). The X-intercept represents the K_i of the inhibitor and error bars indicate standard deviation from three replicate experiments. (B) Increase in absorbance at 388 nm upon addition of PL and ATP. Kinase activity of *St*PLK monitored with PL and ATP for 100 s. 1mg/ml of *St*PLK added after 100 s and 300 s respectively.

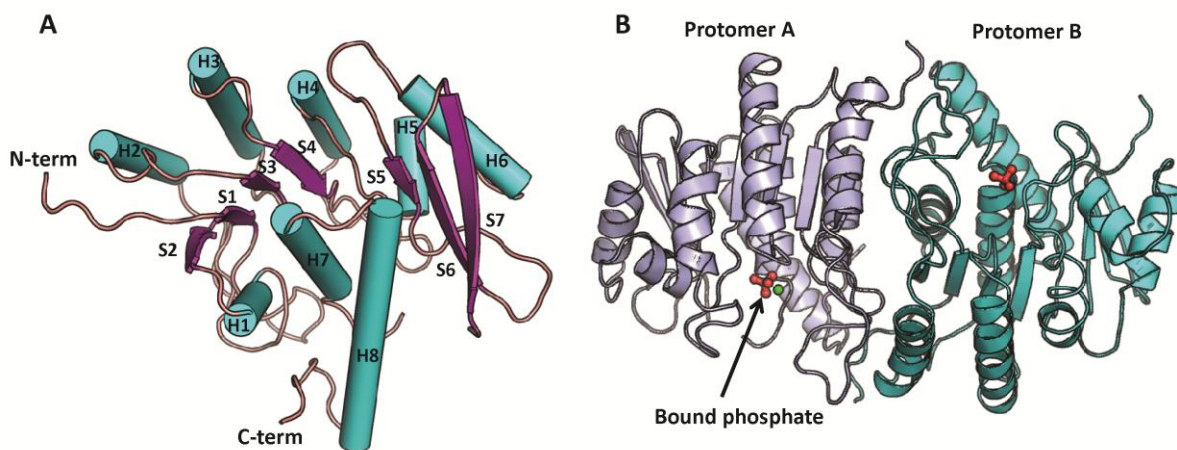


Figure 3. Cartoon representation of *St*PLK structure. (A) The polypeptide fold of *St*PLK protomer. The protomer consists of eight α -helices (H1-H8, cyan cylinder) and seven β -strands (S1-S7, purple arrow). The loops are shown in brown. (B) The biologically active dimeric form of *St*PLK, representing each protomer in a different color. The dimer consists of two independent active sites. The bound phosphate at the active site is shown in orange ball and stick and the Mg^{2+} ion present in one of the protomer is shown as a green ball.

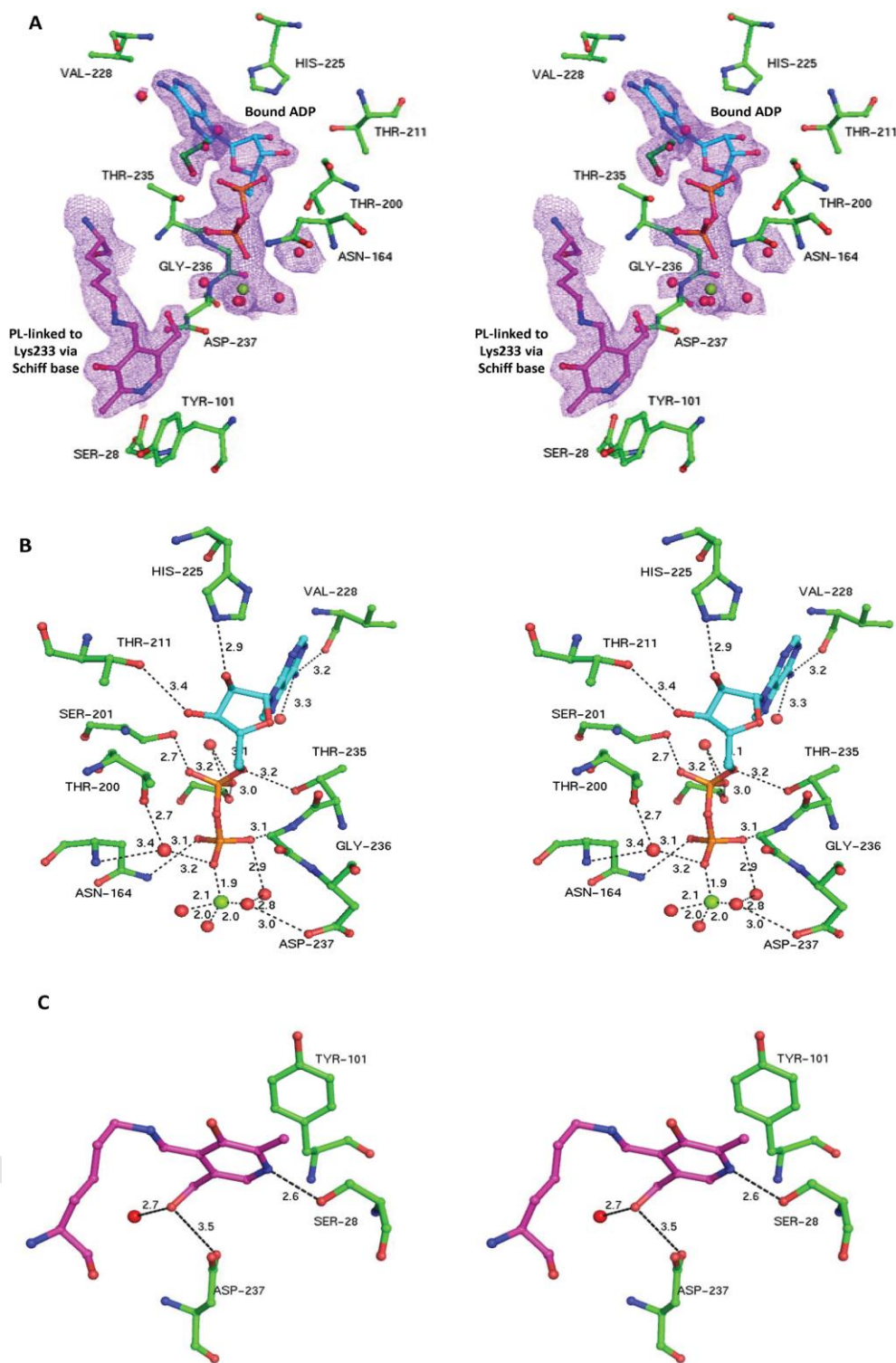


Figure 4. (A) Stereodiagram of the active site of ligand bound *St*PLK (Form I crystal, PDB code: 5ZWA). An ADP molecule (cyan ball and stick) occupies the position corresponding to the ATP binding site of the enzyme. The PL is bound to the active site Lys233 via a Schiff base (purple ball and stick). A Mg^{2+} ion coordinated with a few water molecules occupies the place where γ - PO_4 of ATP binds. The electron density ($2mFo-DFc$ contoured at 1.0σ) for ADP and the Schiff base is shown in blue mesh. (B) The interactions that stabilize the bound ADP (cyan ball and stick) in the active site. The interacting active site residues are shown as

green ball and stick, water molecules as red spheres and Mg^{2+} as a green sphere. The hydrogen bonds are shown as black dash. (C) The interactions between PL (purple ball and stick) and active site residues (green ball and stick). PL forms hydrogen bonding interactions with Ser28, Asp237 and a water molecule (red sphere). PL is also stabilized by π - π stacking interaction with Tyr101.

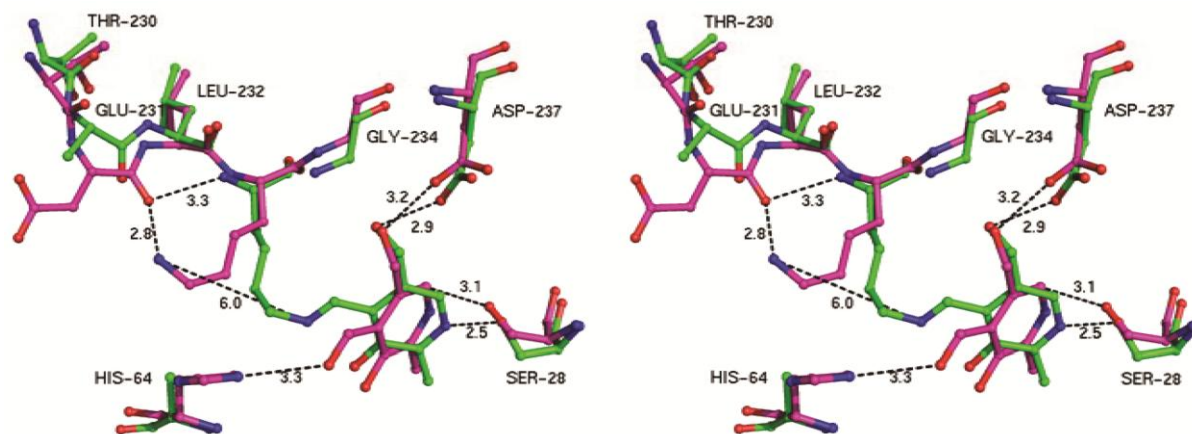


Figure 5. Superposition of the active sites of PL bound *EcDAPAL* (pink ball and stick, PDB code: 2DDW) and *StPLK* Schiff base (green ball and stick, residues are labelled). The PL molecule is stabilized by interactions with nearby His59 and Asp233 in *E. coli* enzyme. However, formation of the Schiff base in *StPLK* leads to the disruption of interaction between PL and the equivalent His64 while retaining the interaction with the Asp237.

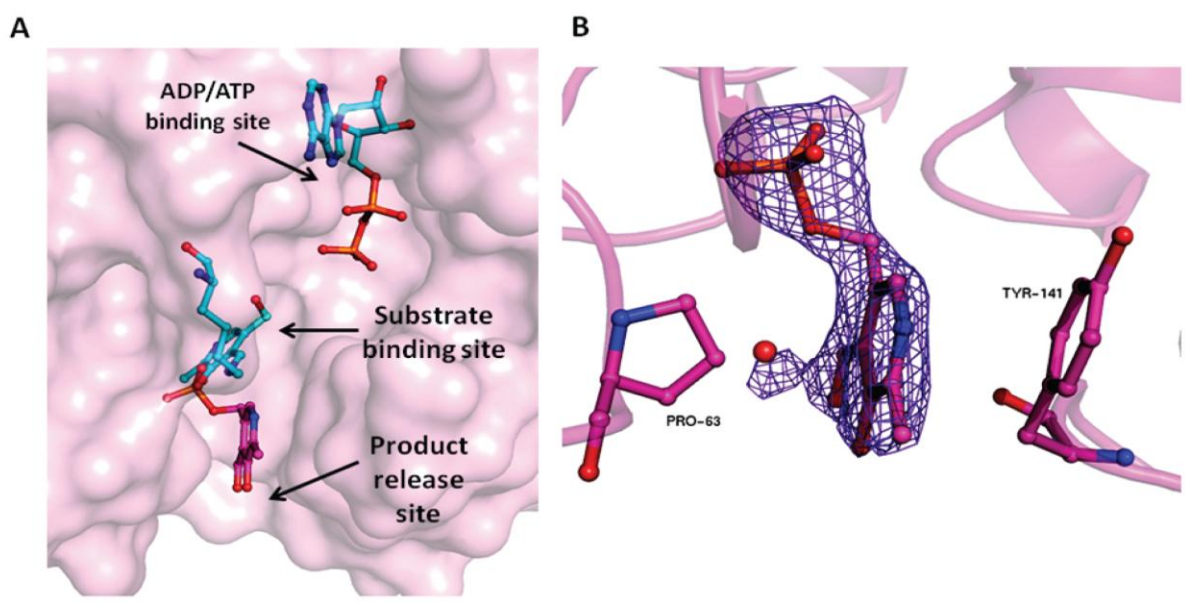


Figure 6. (A) Superposition of the protomer A over protomer B (Form I crystal, PDB code: 5ZWA) achieved using SSM superpose. The protomer B is represented as Pink surface highlighting the product and ligand binding sites. The bound ligands of protomer A (ADP and PL linked via a Schiff base to Lys233, Cyan ball and stick) and PLP (Pink ball and stick) in protomer B are also shown. (B) The PLP in protomer B is hydrogen bonded to a nearby water molecule (red sphere) and held between Tyr141 and Pro63 by non covalent interactions. The electron density (2mFo-DFc contoured at 1.0 σ) for PLP and the water molecule is shown in purple mesh. The PLP is facing away from the substrate binding site, hence representing the product release site.

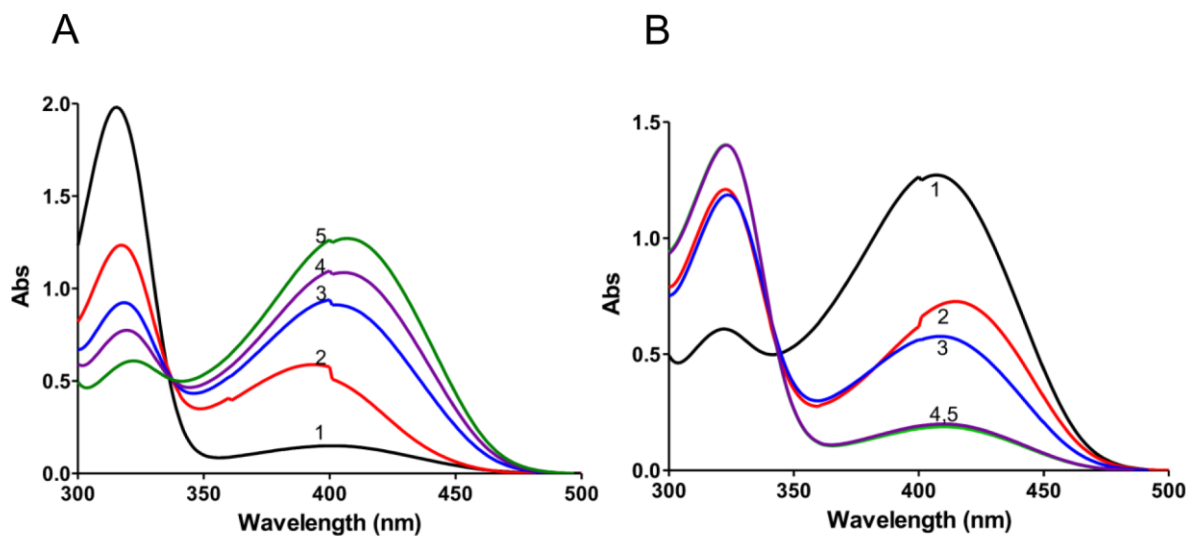
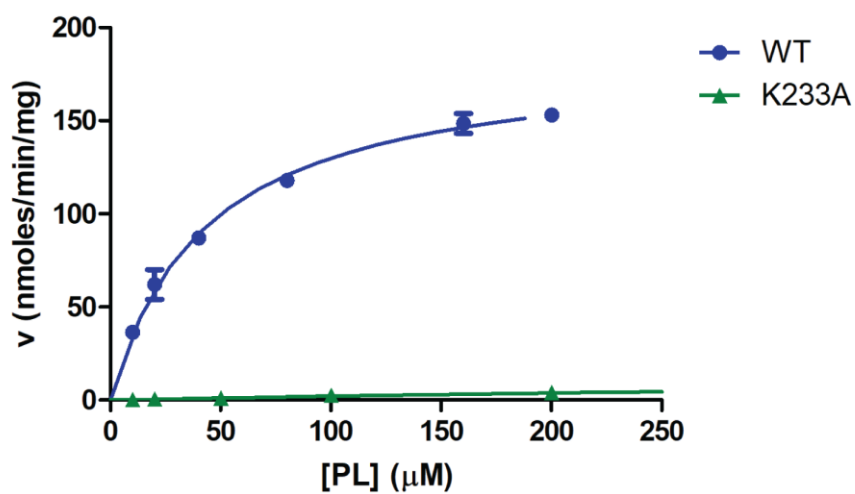
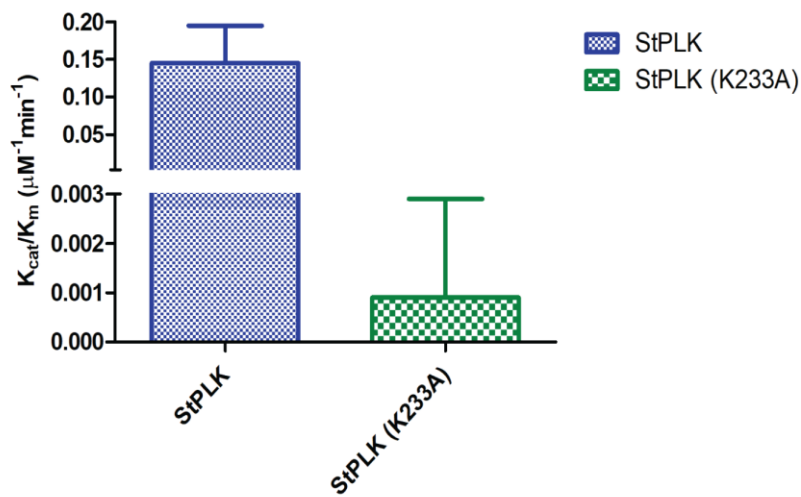


Figure7. Biochemical evidence for the formation of a Schiff base in solution using absorbance spectroscopy. (A) Absorbance spectrum of: 1: *St*PLK (1 mg/ml) with PL (0.3 mM) and $MgCl_2$ (1 mM); 2-5: *St*PLK with PL (0.3 mM), ATP (3 mM) and $MgCl_2$ (1 mM) at 15 sec, 1, 5 and 10 mins of incubation, respectively. An increase in absorbance at 410 nm with time indicates the formation of the Schiff base. (B) Absorbance spectrum of 1: *St*PLK with PL (0.3 mM), ATP (3 mM) and $MgCl_2$ (1 mM); 2-5: *St*PLK with PL (0.3 mM), ATP (3 mM) $MgCl_2$ (1 mM) and 1 mM $NaBH_4$ at 15 sec, 1, 5 and 10 mins of incubation, respectively. The reduction of Schiff base leads to increase in absorbance at 325 nm with a concomitant decrease in absorbance at 410 nm.

A



B



C

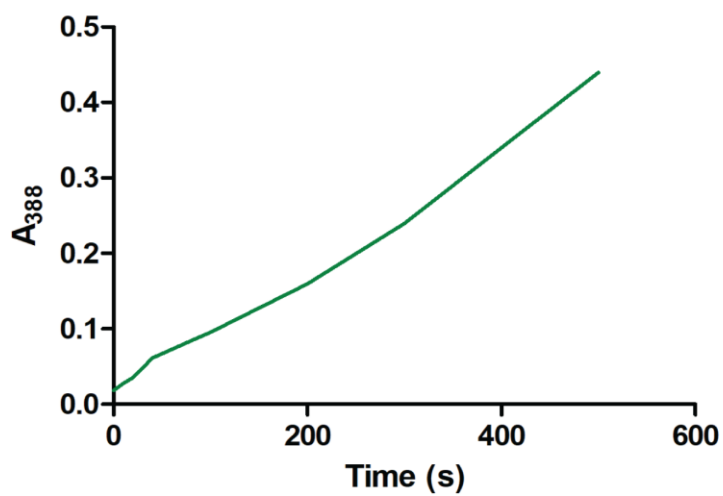


Figure 8. (A) A comparison of catalytic activity of *St*PLK and K233A mutant. 10 $\mu\text{g/ml}$ of *St*PLK and K233A mutant was incubated with varying concentration of PL (0, 10, 20, 40, 80, 160, 200 μM), ATP (1 mM), MgCl_2 (0.7 mM) in 40 mM potassium phosphate buffer (pH 6.6). The assay was carried out in triplicates with three independent preparations of the enzymes and standard deviation was calculated. (B) Bar graph representing the comparative catalytic efficiency (K_{cat}/K_m) of *St*PLK and K233A mutant. (C) Kinase activity of K233A mutant with PL and ATP for 100 s. 1 mg/ml of K233A was added after 100 s and 300 s respectively.

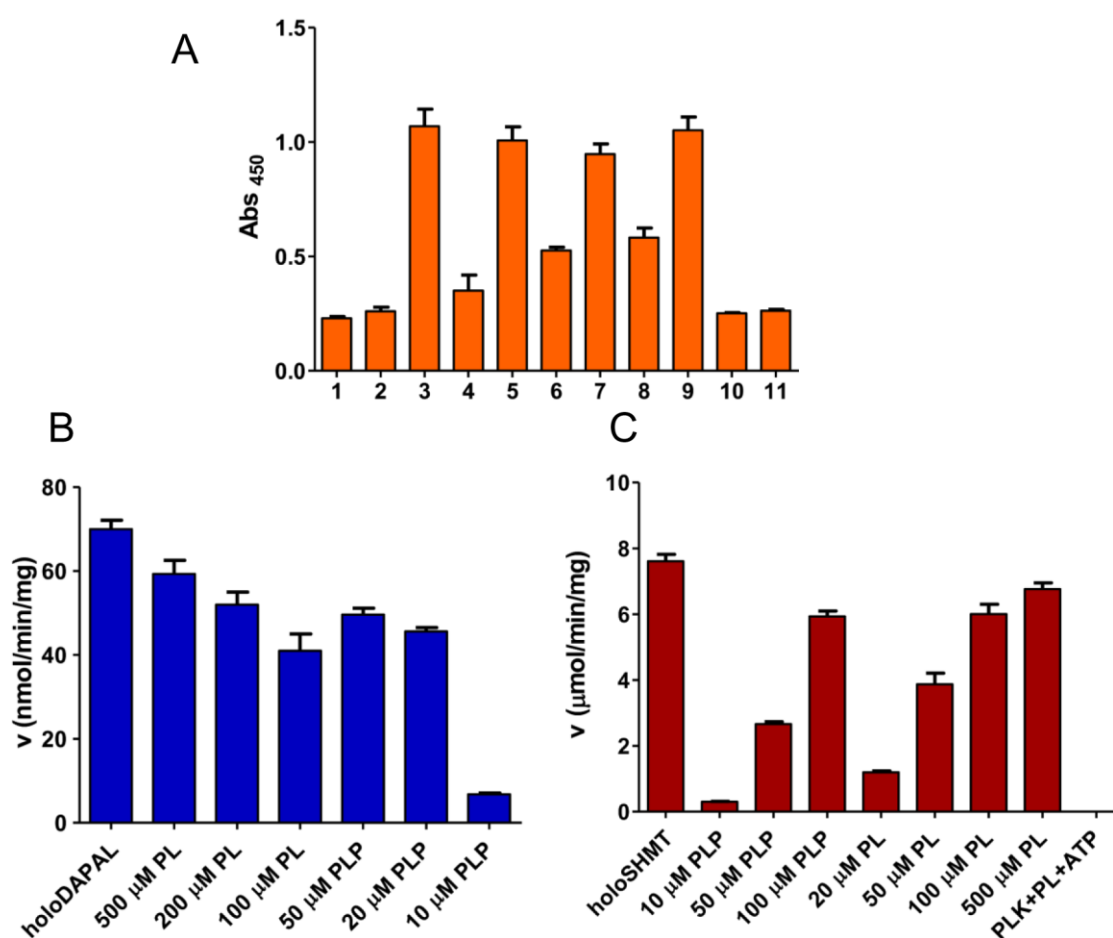


Figure 9. Biochemical studies to detect protein-protein interactions. (A) ELISA based interaction assay of *St*PLK, BSA- BSA + *St*PLK; Buffer- 1xPBS+ *St*PLK; apoSHMT- apo *Bs*SHMT + *St*PLK ; holoSHMT- holo *Bs*SHMT + *St*PLK ; apoCytD- *St*PLK + apo *St*DcytD; holoCytD- *St*PLK + holo *s*DcytD; apoDAPAL- *St*PLK + apo *St*DAPAL; holoDAPAL- *St*PLK + holo *St*DAPAL; PK alone- *St*PLK; SHMT alone- *Bs*SHMT control; CytD alone- *St*DcytD control. The interaction was detected using polyclonal antibody against *St*PLK (second protein) as primary antibody and Goat- anti rabbit IgG coupled to HRP as secondary antibody. The assay was carried out using equimolar concentrations of both the proteins. (B&C) Reconstitution of apo DAPAL and apo *Bs*SHMT using PLK enzymatic activity or addition of PLP externally. (B) Coupled assay for SHMT carried out with apo *Bs*SHMT (3.0

μM) reconstituted by incubation with *St*PLK (3.0 μM), ATP (2 mM), MgCl_2 (0.7 mM) and PL (20-500 μM) or by incubation with PLP (10-100 μM). The assay contained 10 μg of reconstituted *Bs*SHMT and 5 mM L-allothr, 100 μg ADH and 250 μM NADH. (C) Coupled assay for DAPAL carried out with apoDAPAL (3.0 μM) reconstituted by incubation with *St*PLK (3.0 μM), ATP (2 mM), MgCl_2 (0.7 mM) and PL (50-500 μM) (Enzymatic) or by incubation with PLP (5-50 μM) (Non-enzymatic). The assay mixture contained 5 μg of reconstituted *St*DAPAL and 1 mM DL-DAP, 5 units of LDH and 250 μM NADH. Error bars indicate standard deviation from three replicate experiments.